LA-UR-04-5890

Title: USE OF INVERSE SOLUTIONS FOR RESIDUAL STRESS MEASUREMENT

Author(s): Gary S. Schajer (Univ. of British Columbia)
Michael B. Prime (ESA-WR)

Submitted to: Journal of Engineering Materials and Technology
Volume 128, Number 3, July 2006, 375-382

Use of Inverse Solutions for Residual Stress Measurements

Gary S. Schajer

Dept. Mechanical Engineering, University of British Columbia, Vancouver, Canada

Michael B. Prime

Engineering Sciences and Applications Div., Los Alamos National Lab., Los Alamos, NM, USA

Abstract

For most of the destructive methods used for measuring residual stresses, the relationship between the measured deformations and the residual stresses are in the form of an integral equation, typically a Volterra equation of the first kind. Such equations require an inverse method to evaluate the residual stress solution. This paper demonstrates the mathematical commonality of physically different measurement types, and proposes a generic residual stress solution approach. The unit pulse solution method that is presented is conceptually straightforward and has direct physical interpretations. It uses the same basis functions as the Hole-Drilling integral method, and also permits enforcement of equilibrium constraints. In addition, Tikhonov regularization is shown to be an effective way to reduce the influences of measurement noise. The method is successfully demonstrated using data from Slitting (crack compliance) measurements, and excellent correspondence with independently determined residual stresses is achieved.

January 2005

Introduction

A common way of measuring residual stresses in a specimen is to cut away some stressed material and to measure the resulting deformations in the adjacent material. The residual stresses existing in the removed material can then be calculated from the measured deformations, typically displacements or strains. This is the fundamental basis for the "destructive" measurement methods [1]. Commonly used techniques include Sachs' Method [2], Layer Removal [3], Hole-Drilling [4,5], and Slitting (crack compliance) [6,7]. The details of the material removal geometry and the deformation measurements of the various techniques vary greatly. However, the general principle is the same for all methods.

A computational challenge arises when evaluating residual stresses from deformation data from destructive measurements. It occurs because the calculated stresses exist in one region (the removed material) while the measurements are made in a different region (the adjacent material). The measured deformation at a given point in the adjacent material depends on all the stresses within the removed material. Thus, there is not a one-to-one relationship between deformation and residual stress. Instead, the relationship is in the form of an integral equation. This feature profoundly controls the character of the solution.

Even though the various destructive measurement methods differ greatly in their material removal and deformation measurement geometries, the resulting integral equations are almost all generically similar. However, this similarity is not always apparent. Each technique seems to have its own specific calculation method, sometimes not entirely effective. It is the objective of this paper to draw attention to the mathematical commonality of the destructive methods, and to present a generic procedure for achieving effective and reliable solutions.

The proposed solution procedure uses unit pulses as basis functions to solve the integral equations. This method is conceptually straightforward and has direct physical interpretations. The method also permits enforcement of equilibrium constraints. In addition, Tikhonov regularization is used to reduce the influences of measurement noise. The application and effectiveness of the mathematical method is demonstrated using data from Slitting (crack compliance) measurements.

Integral Equations

The relationship between the measured deformations and the residual stresses for a typical destructive method takes the form of an integral equation. For methods based on incremental material removal, this integral is most commonly a Volterra equation of the first kind [8]:

$$d(h) = \int_{h_0}^{h} g(H,h)\ \sigma(H)\ dH \qquad (1)$$

where d(h) is the deformation (displacement or strain) measured when the depth of the removed material equals h. The initial depth h_0 typically equals zero, but may have a non-zero value depending on coordinate system choice. Equation (1) indicates that the measured deformations d(h) depend on the stresses σ originally present at all depths H within the removed material. The kernel function g(H,h) describes the deformation sensitivity to a stress at depth H within removed material of depth h.

Equation (1) is called an "inverse problem" because evaluation of the unknown quantity $\sigma(H)$ requires a solution from left to right. This process is complicated by the appearance of the stress term within the integral. In contrast, the "forward" solution for finding d(h) from a known $\sigma(H)$ can proceed directly from right to left.

The Sachs Boring-Out Method [2] provides an example of a residual stress measurement technique that fits the format of Equation (1). In the Sachs method, relieved strains are measured from strain gages attached to the outside of a cylinder or tube as stressed material is bored out from the center. Traditionally, the stress/strain relations are expressed in differential form:

$$\sigma_\theta(r) = E' \left(\frac{b^2 - r^2}{2r} \frac{d\Psi(r)}{dr} - \frac{b^2 + r^2}{2r^2} \Psi(r) \right) \qquad (2)$$

$$\sigma_a(r) = E' \left(\frac{b^2 - r^2}{2r} \frac{d\Lambda(r)}{dr} - \Lambda(r) \right) \qquad (3)$$

where $E' = E/(1-\nu^2)$ is the plane strain Young's Modulus, and $\psi(r) = \varepsilon_\theta(r) + \nu\, \varepsilon_a(r)$ and $\Lambda(r) = \varepsilon_a(r) + \nu\, \varepsilon_\theta(r)$ are combination strains when the bored out radius reaches r. $\sigma_a(R)$ and $\sigma_\theta(R)$ are

the axial and circumferential stresses at radius R within the removed material. Equations (2) and (3) have the advantage of being "forward" solutions. However, they have the disadvantage of requiring evaluation of differential quantities, which is a calculation well known for error sensitivity, and for not explicitly enforcing equilibrium.

Equations (2) and (3) can be integrated to achieve the format of Equation (1) [9]:

$$\Psi(r) = \int_a^r \frac{2r}{E'\,(b^2 - r^2)}\ \sigma_\theta(R)\ dR \tag{4}$$

$$\Lambda(r) = \int_a^r \frac{2}{E'\,(b^2 - r^2)}\ \sigma_a(R)\ R\,dR \tag{5}$$

where b is the outside radius and a is the initial inside radius. An undesirable feature of these equations is the presence of the denominator term b^2-r^2. It creates a singularity by zero division at r = b, and a large range of kernel function values for r < b. This large range of values makes practical solutions of Equations (4) and (5) ill-conditioned and sensitive to round-off errors. The problem can be avoided by noting that the denominator term does not involve the integrand R, and therefore can be factored out of the integrals. Transferring the denominator term to the left side removes its ill effects. With this change, Equations (4) and (5) become:

$$d_\theta(r) = \frac{E'(b^2 - r^2)\,\Psi(r)}{2\,b^2} = \int_a^r \frac{r}{b^2}\ \sigma_\theta(R)\ dR \tag{6}$$

$$d_a(r) = \frac{E'(b^2 - r^2)\,\Lambda(r)}{2\,b^2} = \int_a^r \frac{R}{b^2}\ \sigma_a(R)\ dR \tag{7}$$

These equations retain the form of Equation (1), with the "data" terms d_θ and d_a becoming scaled quantities. The corresponding kernel functions behave smoothly and remain within a compact range, even at r = b. Consequently, they give numerical solutions that are much better conditioned than the theoretically equivalent Equations (4) and (5). The additional factors E'/b^2 are included so that the kernel function integrals are dimensionless. This feature assists with numerical tabulations of the kernel function integrals when needed for practical calculations.

At r = b the left sides of Equations (4) and (5) equal zero. The associated right sides are recognized as the circumferential and axial force equilibrium conditions:

$$d_\theta(b) = 0 = \int_a^b \sigma_\theta(R)\ dr \tag{8}$$

$$d_a(b) = 0 = \int_a^b \sigma_a(R)\ R\ dr \tag{9}$$

The additional term R occurs in Equation (9) because of the circular geometry. For other geometries, an additional term analogous to R indicates moment equilibrium.

Similar equations apply to the Layer Removal Method. In this case, measurements are made from strain gages attached to a planar specimen as layers of stressed material are removed from the opposite face [3]. The combination strain $\Gamma(h) = \varepsilon_x(h) + \nu\ \varepsilon_y(h)$ measured when the depth of removed material reaches h is [10]:

$$\Gamma(h) = \int_0^h \left[\frac{6H - 2W - 4h}{E'\ (W - h)^2}\right]\ \sigma(H)\ dH \tag{10}$$

where σ is the stress at depth H, and W is the original plate thickness. Analogous to the Sachs Equations (4) and (5), the denominator term $(W-h)^2$ creates a singularity in Equation (10) by zero division at h = W. As before, this singularity can be removed by factoring the term out of the integral and transferring it to the left side of the equation. The result is:

$$d_h(h) = \frac{E'\ (W - h)^2\ \Gamma(h)}{W^2} = \int_0^h \frac{6H - 2W - 4h}{W^2}\ \sigma(H)\ dH \tag{11}$$

For the extreme case when h = W, the left side of Equation (11) equals zero. The right side then corresponds to moment equilibrium:

$$d_h(W) = 0 = \int_0^W (H - W)\ \sigma(H)\ dH \tag{12}$$

For Hole-Drilling and Slitting measurements, integral equations of the form of Equation (1) also apply. However, because of the more complex geometries involved, the corresponding kernel functions cannot be determined analytically. Instead, the kernel functions are evaluated numerically using finite element calculations [11,12]. Slitting measurements are analogous to

Layer Removal measurements, and have a singularity when the slit depth h approaches the full plate thickness W. This singularity can similarly be avoided by multiplying the measured strains and the kernel function by the factor $E' (W-h)^2 / W^2$.

The generic similarity of the various residual stress measurement methods can be seen clearly by comparing their kernel functions. In the next section, it will be shown that the integral of the kernel function is a useful quantity. Figure 1 shows the integrals of the dimensionless kernel functions for the Sachs, Layer Removal, Hole-Drilling and Slitting methods. The close similarity of these diagrams is quite remarkable given the wide differences in the practical details of the different methods. This similarity motivates the objective of the present work to develop a generic residual stress calculation method that will give effective and reliable results for a wide range of destructive measurement techniques.

Solution Method

An effective way of solving an inverse equation such as Equation (1) is to express the unknown function, here the stress profile $\sigma(H)$, as the sum of a series of basis functions $u_i(H)$ multiplied by coefficients c_i to be determined [7].

$$\sigma(H) = \sum c_i \, u_i(H) \tag{13}$$

The solution involves determining the coefficient values c_i. The basis functions $u_i(H)$ must be linearly independent and their combination must be able to represent the solution adequately. Possible choices include unit pulses [11,13,14], power series [11], and Legendre polynomials [6,9]. Each of these choices has advantages and disadvantages. The unit pulses and power series are conceptually and algebraically straightforward. However, they do not automatically obey equilibrium. Conversely, Legendre polynomials do automatically obey equilibrium, but they are more complex to implement.

Here, unit pulses are chosen as basis functions because they are conceptually straightforward. They directly use the kernel function data in Figure 1 to obtain their deformation vs. stress calibration. Figure 2 graphically shows a series of unit pulse functions. The width of each pulse corresponds to successive increments in material removal depth, which

are not necessarily all equal. The deformations are measured after each material removal increment. For unit pulses, the coefficients c_i is Equation (13) correspond to the stresses σ_i within each material increment. Thus, it is convenient to rename the generic coefficients c_i in Equation (13) with the specific notation σ_i. The symbol σ_i will be used in place of c_i in all following equations.

Substitution of unit pulse functions into Equations (1) and (13) yields the matrix equation:

$$\mathbf{G}\,\boldsymbol{\sigma} = \mathbf{d} \tag{14}$$

where

$$\mathbf{d} = \mathbf{F}\,\boldsymbol{\varepsilon} \tag{15}$$

and

$$G_{ij} = \int_{h_{j-1}}^{h_j} g(H,h_i)\ dH = \int_{h_0}^{h_j} g(H,h_i)\ dH - \int_{h_0}^{h_{j-1}} g(H,h_i)\ dH \tag{16}$$

In Equation (14), the left-side (solution) vector $\boldsymbol{\sigma}$ corresponds to the stresses within each of the increments. The right-side (data) vector **d** corresponds to the set of deformation measurements $\boldsymbol{\varepsilon}$ made after each material removal increment. For example, these "deformation measurements" could represent the combination strains $\Psi(r)$, $\Lambda(r)$ or $\Gamma(h)$ in Equations (4), (5) or (10). For the Sachs and Layer Removal methods, **F** in Equation (15) is a matrix with $E'(b^2-r_i^2)/2b^2$ or $E'(W-h_i)^2/W^2$ along its diagonal.

The coefficients G_{ij} in Equation (16) are the differences of integrals of the kernel function for the particular residual stress measurement method. The format of this equation is chosen because each integral term in the right is a function of only two variables, h_i and h_j. This feature makes it easy to tabulate and interpolate these integrals to obtain practical numerical values of G_{ij}. If Equation (16) had been expressed in the more compact form achieved by combining the two integrals into a single integral spanning h_{j-1} to h_j, a more complex three-variable interpolation would have been needed Figure 1 shows some example contour plots of the integrals, while Figure 3 schematically shows the physical meaning of the matrix terms on the left of Equation (16) for the case of Hole-Drilling (and analogously for the other methods). Coefficient G_{ij} is seen to correspond to the deformation caused by a stress within increment "j"

of a hole that is "i" increments deep. Because the deformations are sensitive only to stresses within the removed material, non-zero values of G_{ij} occur only when $j \leq i$. Thus, **G** is lower triangular. For Hole-Drilling and some implementations of other methods, Equation (14) is sufficient to provide a solution for the residual stresses within each depth increment. In this case, it corresponds to the "Integral Method" [11].

Equilibrium

With several residual stress measurement methods, e.g., Sachs' method, Layer Removal and Slitting, the material removal can proceed through almost the entire thickness of the material. In such cases, enforcement of equilibrium becomes an additional need. This constraint can be achieved by expanding Equation (14) by an additional row corresponding to the theoretical extreme case of complete material removal. This row corresponds to an equilibrium equation such as (8), (9) or (12). The additional row determines the stress in the ligament remaining after completion of material removal.

$$\begin{bmatrix} G_{11} & & & \\ G_{21} & G_{22} & & \\ G_{31} & G_{32} & G_{33} & \\ G_{41} & G_{42} & G_{43} & G_{44} \end{bmatrix} \begin{bmatrix} \sigma_1 \\ \sigma_2 \\ \sigma_3 \\ \sigma_4 \end{bmatrix} = \begin{bmatrix} d_1 \\ d_2 \\ d_3 \\ 0 \end{bmatrix} \tag{17}$$

Equation (17) shows an example where deformation measurements d_i have been made after three material removal increments. The fourth (additional) row has a zero on the right side, and enforces equilibrium. σ_1, σ_2, σ_3 are the stresses within the three material removal increments, and σ_4 is the stress within the remaining ligament. For meaningful results, the thickness of the remaining ligament should be similar to that of the material removal increments. If this is not the case, the estimate of the stress in the remaining ligament may not be realistic, and Equation (14) should be used to estimate the stresses within the removed material only.

The above method of adding an extra row to Equation (14) is effective when only one equilibrium condition needs to be enforced. This is the case when using the Sachs method. However, for Layer Removal and Slitting, both force and moment equilibrium apply, but only moment equilibrium is enforced by the additional row in Equation (17). The method of

Lagrange multipliers [14] can be used to add the force equilibrium constraint. However, it does this at the cost of disturbing the moment equilibrium condition contained in the added row in Equation (17). There is only the one independent stress available in the remaining ligament, so it cannot be chosen to enforce two equilibrium conditions simultaneously.

The force equilibrium procedure suggested here is first to compute the stresses $\boldsymbol{\sigma}$ using Equation (17), or the regularized solution to be described in the next section. Then compute the force residual corresponding to those stresses. The size of this force residual provides a measure of the quality of the measured data. The corresponding "average stress" should be much smaller than the maximum calculated stress, preferably less than 1%. This average stress can then be subtracted from the previously calculated stresses to give an "adjusted" stress profile that obeys force equilibrium.

Regularization

All practical data are a combination of "true data" and measurement noise. The noise component causes local distortions that produce proportionally larger distortions in the computed stress solution. For solutions using pulse functions, the noise amplification is usually kept small by using only a few unevenly spaced material removal increments [11,16]. This approach is effective, but it diminishes the data content of the calculation, and decreases the spatial resolution of the stress solution.

The opposite approach is taken here, where the data content of the calculation is increased by using displacements measured while making a large number of material removal increments. The resulting noise amplification is ameliorated by using Tikhonov regularization [17]. This procedure effectively smoothes the stress solution [18,19]. It diminishes the adverse effect of the noise without significantly distorting the part of the stress solution corresponding to the "true data".

The Tikhonov method involves modifying Equation (17) to penalize the local extreme values in the stress solution that occur because of the presence of noise. The penalty can be applied to the norm of the stresses, thereby creating a "small" solution. Alternatively, it may be

applied to the norms of the first or second derivatives of the stresses, thus creating a "flat" or "smooth" solution. In general, any combination of penalty types may be used.

Penalization of the extreme values associated with measurement noise alters the stress solution such that it no longer exactly obeys Equation (17). Consequently, there is a misfit between the measured data **d** and the data corresponding to the regularized solution **σ**. The regularized stresses do not include any influence from the misfit. Therefore, the misfit should ideally contain mostly noise, and very little true data. The amount of regularization should be chosen to achieve this objective; it should be sufficiently large to reduce substantially the artifacts created by the noise, but not so large as to distort significantly the structure of the true solution.

When implementing Tikhonov regularization, Equation (17) is pre-multiplied by $\mathbf{G}^T$ and augmented by an extra term. The result is:

$$(\mathbf{G}^T\mathbf{G} + \beta\,\mathbf{C}^T\mathbf{S}^T\mathbf{H}\,\mathbf{S}\,\mathbf{C})\;\boldsymbol{\sigma} = \mathbf{G}^T\mathbf{d} \tag{18}$$

where matrix **C** evaluates the chosen derivative of the stress solution that is to be penalized. For "small", "flat" or "smooth" solutions, **C** numerically approximates the zeroth, first or second derivatives respectively. For evenly spaced data, **C** contains rows (0,1,0), (0,-1,1) or (-1,2,-1) centered along its main diagonal. For residual stress calculations, "smooth" (second derivative) regularization is a good choice because it does not significantly disturb force or moment equilibrium. For uniformly spaced data, the matrix product **H S C** has the following structure

$$\mathbf{H}\,\mathbf{S}\,\mathbf{C} = \begin{bmatrix} (h_1 - h_0)/W & & & \\ & (h_2 - h_1)/W & & \\ & & (h_3 - h_2)/W & \\ & & & (h_4 - h_3)/W \end{bmatrix} \begin{bmatrix} s_1 & & & \\ & s_2 & & \\ & & s_3 & \\ & & & s_4 \end{bmatrix} \begin{bmatrix} 0 & 0 & 0 & 0 \\ -1 & 2 & -1 & 0 \\ 0 & -1 & 2 & -1 \\ 0 & 0 & 0 & 0 \end{bmatrix} \tag{19}$$

where the first and last rows of **C** are set to zero to eliminate the small and flat regularization that an "incomplete" (-1 2 –1) pattern would produce at the end points. For example, a non-zero row sum indicates small regularization. For non-uniformly spaced data, the rows *i = 2, N-1* of matrix **C** have the following tridiagonal structure:

$$\frac{-2\,(W/N)^2}{(h_{i+1} - h_{i-1})(h_i - h_{i-1})} \qquad \frac{2\,(W/N)^2}{(h_i - h_{i-1})(h_{i+1} - h_i)} \qquad \frac{-2\,(W/N)^2}{(h_{i+1} - h_i)(h_{i+1} - h_{i-1})} \tag{20}$$

Matrix **S** in Equations (18) and (19) contains along its main diagonal the standard errors s_i in the deformation data d_i. This matrix adjusts the amount of regularization to fit the expected measurement error of each deformation datum d_i.

In Equations (18), β is a weighting factor called the regularization parameter. $\beta = 0$ indicates no regularization, and $\beta > 0$ indicates an increasing amount of regularization. The Morozov Discrepancy Principle [17] can be used to determine the value of β that gives the optimal regularization that substantially reduces noise without significantly distorting the true solution. If the noise in the data are Gaussian with zero mean, the Morozov principle specifies that the optimal value of β is achieved when the chi-squared statistic, χ^2, equals the number of data points N. Here, this corresponds to

$$\chi^2 \quad = \quad \sum_{i=1}^{N} \left(\frac{d_i^{calc} \; - \; d_i^{meas}}{s_i} \right)^2 \quad = \quad \left\| \mathbf{S}^{-1} \left(\mathbf{G\sigma - d} \right) \right\| \quad = \quad N \tag{21}$$

where d_i^{meas} are the measured deformation data, and d_i^{calc} are the deformation data corresponding to the regularized σ_j that are calculated using Equations (1) and (15).

In many practical cases, the situation is complicated by the presence of matrix **F** in Equation (15). A strain quantity $\boldsymbol{\varepsilon}$ is actually measured, and is then mathematically transformed into the data quantity **d** for use in the subsequent calculations. When working in terms of $\boldsymbol{\varepsilon}$ Equation (21) becomes

$$\chi^2 \quad = \quad \sum_{i=1}^{N} \left(\frac{\varepsilon_i^{calc} \; - \; \varepsilon_i^{meas}}{e_i} \right)^2 \quad = \quad \left\| \mathbf{E}^{-1} \left(\mathbf{F}^{-1}\mathbf{G\sigma - \varepsilon} \right) \right\| \quad = \quad N \tag{22}$$

where e_i are the standard errors in the measured strains. Commonly, the measured strains have a uniform standard error, $e_i = e$ for all i. Equation (22) can then be rearranged as:

$$\frac{\left\| \mathbf{F}^{-1}\mathbf{G\sigma - \varepsilon} \right\|}{N} \quad = \quad e^2 \tag{23}$$

In this simplified case, the Morozov discrepancy principle is seen to match the mean square data misfit to the standard error in the measured data.

When enforcing equilibrium, there are no measured data associated with the material in the last (remaining) layer. Thus, the last line of the matrix calculation in Equation (23) must be

omitted and N reduced to N-1. The pre-multiplication by $\mathbf{F}^{-1}$ is simply done by dividing the elements of $\mathbf{G\sigma}$ by f_i. Omission of the last line of the matrix calculation avoids the zero division by the final $f_n = 0$.

For the case of uniform strain measurement errors $e_i = e$ for all i, the corresponding matrix **S** has the same form as **F**, but with the elements multiplied by a factor containing E'. Consequently, it is acceptable to replace **S** in Equation (18) with **F**, and absorb the factor into β.

If e is known, then the optimally regularized solution can be determined by finding the value of β that simultaneously solves Equations (18) and (23). This solution can be found iteratively. However, in practice, the standard error e is usually not reliably known. Values previously determined by the measurement equipment manufacturer or user may not apply to the specific circumstances of the particular measurement. Thus, a systematic method is needed to estimate the standard measurement error within the given data. The approach suggested here is to assume that the "true data" have slowly varying curvature on a spatial scale that is large compared with the depth increments used for the data measurement. Thus, any shape feature in the true data profile is spanned by several measurements. Under these conditions, any more rapidly varying changes in the measured data can be assumed to be noise.

A convenient method to separate slowly and rapidly varying features in the measured strains is to consider the data in groups of four adjacent points. A least-squares parabola is evaluated that passes among successive sets of four points. The least-squares solution is needed because a parabola does not in general exactly fit more than three data points. However, if there were no data noise, the parabola would likely fit the smooth "true data" quite well, and there would be almost no misfit between the curve and the four points. Thus, with noisy data, the misfit could be mostly attributed to the noise. It may be shown that for strain data taken at four equal depth increments, the local misfit norm is

$$\text{local misfit norm} \quad = \quad \frac{1}{20}\left(\varepsilon_1 - 3\varepsilon_2 + 3\varepsilon_3 - \varepsilon_4\right)^2 \tag{24}$$

For the case where all the standard errors are the same, i.e., $s_i = s$, then the standard error can be estimated using

$$e^2 \approx \frac{1}{20(N-3)} \sum_{i=1}^{N-3} \left(\varepsilon_i - 3\varepsilon_{i+1} + 3\varepsilon_{i+2} - \varepsilon_{i+3}\right)^2 \quad (25)$$

Although it is not exact, the estimated value of e^2 is useful as a starting value for choosing a reasonable amount of regularization when solving Equations (18) and (23). Sometimes, it may be necessary to adjust the estimate if the resulting regularization is either insufficient to remove noise artifacts, or is excessive in distorting the true solution.

Practical Example

The mathematical procedure described in the previous sections was applied to the data from a Slitting experiment on a known-stress specimen. To prepare the specimen, strain gages were attached to the top and bottom of a stress-relieved stainless steel beam, 30.0mm deep. Residual stresses were induced in the beam by loading it into the plastic range using a four-point bend fixture. On removal of the load, the beam unloaded elastically, leaving permanent plastic deformations and substantial axial residual stresses. During this loading and unloading, the total load and corresponding strains were measured. The profile of the residual stresses was calculated from the measured strain data using the stress-strain curve identification method described by Mayville and Finnie [20]. Before destructive measurement by Slitting, the residual stresses in the beam were measured by neutron and x-ray diffraction, and within the associated uncertainty ranges, the results agreed with those of the stress-strain curve calculation [21].

Following the creation and evaluation of the residual stresses, the beam was mounted in a wire electro-discharge machine that progressively cut a slit extending from one surface of the beam almost all the way to the opposite surface. A 200 μm diameter hard brass wire was used for the cutting, which was performed using "skim cut" settings so that only negligible stresses would be induced. The cutting was done in 36 steps, at approximately 0.8mm intervals to a final depth of 29.26 mm, 97.5% of the beam depth. The cut depth and the strain measured by a strain gage mounted on the opposite surface were recorded at the completion of each step. After cutting, the width of the cut was measured as 267 μm.

Figure 4 shows the measured strains vs. cut depth. The measurements were quite stable, with minimal noise. The standard error in the strain measurements was estimated using Equation (25) as 0.7 micro-strain. The last two strains were omitted in this calculation because they had apparent errors substantially larger than the others. These errors likely occurred because it was difficult to support the very flexible remaining ligament without introducing any external loads. The corresponding residual stresses were calculated by iteratively solving Equations (18) and (23).

Finite element calculations were used to generate the data for matrix **G**. The calculations followed a standard procedure using finite elements [12], with pulse functions being used here as basis functions instead of the polynomials previously used. The mesh was a 2-D plane-strain mesh of quadratic shape function quadrilaterals. The mesh included the finite slit width. The elastic modulus of the stainless steel was taken as 194 GPA, measured during the bending, and Poisson's ratio was taken as 0.28 from reported values. In Figure 1(d), the function values at the extreme limit corresponding to a slit depth exactly equal to the specimen total depth were determined by assuming an analogy to Equation (11) for Layer Removal. These values correspond to moment equilibrium, as indicated in Equation (12). Figure 5 shows the residual stress profile calculated using Equations (18) and (23), and the profile calculated from the strains measured during the bend test. The stresses are plotted at the midpoint of each interval and connected by straight lines. The two profiles are almost identical. This excellent correspondence gives strong confidence in the applicability of the numerical method described here and of the stress-strain curve identification method of Mayville and Finnie [20]. In addition, the stress residual required to achieve a zero force resultant is 1.3 MPa, which is just over 1% of the maximum observed stress values. This small size of this residual gives further confidence in the results. To achieve the best estimate of the actual solution, the Equation (18) profile plotted in Figure 5 includes an *a-posteriori* subtraction of the stress residual.

Figure 6 shows residual stress profiles calculated using three different amounts of regularization: insufficient, optimal (corresponding to Figure 5), and excessive. These respectively correspond to misfit norms of a tenth, equal and ten times the optimal value of 0.7 micro-strain. In this case, where the data are high quality, with only modest measurement errors, the sensitivity to the amount of regularization is not large. This is not necessarily a general

behavior. The under-regularized stress profile has oscillations on the left side, but has a sharp curve at the first stress peak. The over-regularized stress profile does not have the initial oscillations, but it excessively smoothes the first stress peak. The optimally regularized stress profile mostly avoids the initial oscillations while still giving a sharp curve at the first stress peak.

Figure 7 shows the strain misfits corresponding to the calculated residual stress profiles in Figure 6. Regularization is seen to act like a low-pass filter. With insufficient regularization, the misfit contains a small amount of high frequency noise. With increased (optimal) regularization, the misfit also takes in some lower frequency noise, and therefore grows in size. The shape is still quite random, and likely mostly contains measurement noise. With excessively large regularization, the misfit takes in a yet lower frequency component with wavelengths spanning several data points. This non-random structure indicates that the increase was taken mostly from the "true solution" rather than from the remaining measurement noise.

Discussion

Although not apparent in this example, the computed stress value at the right end of the residual stress curve in Figure 5 can be sensitive to data errors. This last value corresponds to the stress in the ligament remaining after the last cut. The error sensitivity occurs because the last stress value has no data of its own, but is calculated using moment equilibrium from all the other data. Thus, the last stress is forced to compensate for most of the accumulated errors in all the other stresses. When working with non-ideal data, more realistic results may be achieved by disabling moment equilibrium enforcement by setting the last row of matrix **G** in Equation (17) to zero. The presence of regularization allows Equation (18) to continue to give a solution for the stress in the remaining ligament. In this case, the result is essentially an extrapolation of the adjacent stress values. If desired, an *a-posteriori* moment equilibrium correction can be made in the same way as a force equilibrium correction.

When seeking solutions from inverse equations such as those presented here, it is important to be realistic in ones expectations. Inverse equations are very sensitive to data noise, and they rarely give well-defined solutions of the type provided by "forward" equations. In

some ways, the "solution" to an inverse equation can be considered as a "best guess." The solution process is analogous to someone trying to guess the contents of a wrapped gift by squeezing the wrapping paper. If the wrapping is very thin (low measurement noise) the shape of the contents can be probed in some detail, and a realistic conclusion can be made about the gift. However, as the wrapping gets thicker (increased measurement noise), the ability to probe the shape of the contents and make a realistic conclusion progressively deteriorates. With these ideas in mind, it is clear that high quality data form a primary requirement. Meticulous experimental technique is therefore essential for getting reliable results.

Conclusions

For most of the destructive methods used for measuring residual stresses, the relationship between the measured deformations and the residual stresses are in the form of an integral equation. Such equations require an inverse method to evaluate the residual stress solution.

This paper demonstrates the mathematical commonality of physically different measurement types, thereby permitting a generic residual stress solution approach. The unit pulse solution method presented here is conceptually straightforward and has direct physical interpretations. It also permits enforcement of equilibrium constraints. The method is successfully demonstrated using data from Slitting measurements, and excellent correspondence with independently determined residual stresses is achieved. In addition, Tikhonov regularization is shown to be an effective way to reduce the influences of measurement noise. When working with non-ideal data, it may be desirable to enforce equilibrium after, rather than within, the stress calculation.

Acknowledgments

This work was financially supported by the Natural Sciences and Engineering Research Council of Canada (NSERC) and by the Los Alamos National Laboratory, NM, USA, operated by the University of California for the United States Department of Energy under contract W-7405-ENG-36.

References

1. Schajer, G. S., 2001, "Residual Stresses: Measurement by Destructive Testing." Encyclopedia of Materials: Science and Technology, Elsevier, pp.8152-8158.

2. Sachs, G., and Espey, G., 1941, "Measurement of Residual Stresses in Metal." Iron Age, Sept. 18, pp.63-71; Sept. 25, pp.36-42.

3. Treuting, R. G., and Read, W. T., 1951, "A Mechanical Determination of Biaxial Residual Stress in Sheet Materials," Journal of Applied Physics, **22**(2), pp.130-134.

4. American Society for Testing and Materials, 1999, "Standard Test Method for Determining Residual Stresses by the Hole-Drilling Strain Gage Method." Standard E837-99. American Society for Testing and Materials, West Conshohocken, PA

5. Measurements Group, 1993, "Measurement of Residual Stresses by the Hole Drilling Strain-Gage Method," Tech Note TN-503-5, Measurements Group, Raleigh, NC, 20 pp.

6. Cheng, W., and Finnie, I., 1986, "Measurement of Residual Hoop Stress in Cylinders Using the Compliance Method," Journal of Engineering Materials and Technology, **108**, pp.87-92.

7. Prime, M. B., 1999, "Residual Stress Measurement by Successive Extension of a Slot: The Crack Compliance Method," Applied Mechanics Reviews, **52**(2), pp.75-96.

8. Parker, R. L., 1994, "Geophysical Inverse Theory," Princeton University Press, New Jersey.

9. Lambert, J. W., 1953, "A Method of Deriving Residual Stress Equations," Proceedings SESA, **12**(1), pp.91-96.

10. Virkar, A. V., 1990, "Determination of Residual Stress Profile Using a Strain Gage Technique," Journal of the American Ceramic Society, **73**(7), pp.2100-2102.

11. Schajer, G. S., 1988, "Measurement of Non-Uniform Residual Stresses Using the Hole-Drilling Method," Journal of Engineering Materials and Technology, **110**(4), Part I: pp.338-343, Part II: pp.344-349.

12. Rankin, J. E., Hill, M. R., and Hackel, L. A., 2003, "The Effects of Process Variations on Residual Stress in Laser Peened 7049 T73 Aluminum Alloy," Materials Science and Engineering *A*, **A349**, pp.279-291.

13. Bijak-Zochowski, M., 1978, "A Semi-destructive Method of Measuring Residual Stresses," VDI-Berichte, **312**, pp.469-476.

14. Ritchie, D., and Leggatt, R. H., 1987, "The Measurement of the Distribution of Residual Stresses Through the Thickness of a Welded Joint," Strain, **23**(2), pp.61-70.

15. Dahlquist, G., Björck, Å., and Anderson, N., 1974, "Numerical Methods," Prentice-Hall, Englewood Cliffs.

16. Vangi, D., 1994, "Data Management for the Evaluation of Residual Stresses by the Incremental Hole-Drilling Method," Journal of Engineering Materials and Technology, **116**(4), pp.561-566.

17. Tikhonov, A., Goncharsky, A., Stepanov, V., and Yagola, A., 1995, "Numerical Methods for the Solution of Ill-Posed Problems," Kluwer, Dordrecht.

18. Liu, X., and Schajer, G. S., 1997, "More Reliable Calculations for Layer-Removal Residual Stress Measurements," Proceedings of SEM Spring Conference on Experimental Mechanics, pp.255-256.

19. Tjhung, T., and Li, K., 2003, "Measurement of In-plane Residual Stresses Varying with Depth by the Interferometric Strain/Slope Rosette and Incremental Hole-Drilling," Journal of Engineering Materials and Technology, **125**(2), pp.153-162.

20. Mayville, R. A., and Finnie, I., 1982, "Uniaxial Stress-Strain Curves from a Bending Test." Experimental Mechanics, **41**(2), pp.197-201.

21. Prime, M. B., *et al.,* 1998, "Several Methods Applied to Measuring Residual Stress in a Known Specimen," Proc. SEM Spring Conference on Experimental and Applied Mechanics, Houston, Texas, pp.497-499.

List of Figures

1. Contour plots of kernel function integrals. (a) Sachs' Method, (b) Layer Removal, (c) Hole-Drilling [11], (d) Slitting.

2. Unit pulse functions used for the residual stress solution.

3. Physical interpretation of matrix coefficients G_{ij} for the Hole-Drilling method.

4. Strain vs. slit depth for a residual stress measurement using the Slitting method.

5. Residual stress profiles. Solid line = calculated from Fig.4 data using Equations (18) and (23). Dashed line = calculated from bending strains.

6. Residual stress profiles calculated using different amounts of regularization. Misfit norms = 0.07, 0.7 (optimal) and 7.0 micro-strain.

7. Strain misfits calculated using different amounts of regularization.
Misfit norms: (a) = 0.07, (b) = 0.7 (optimal), and (c) = 7.0 micro-strain.

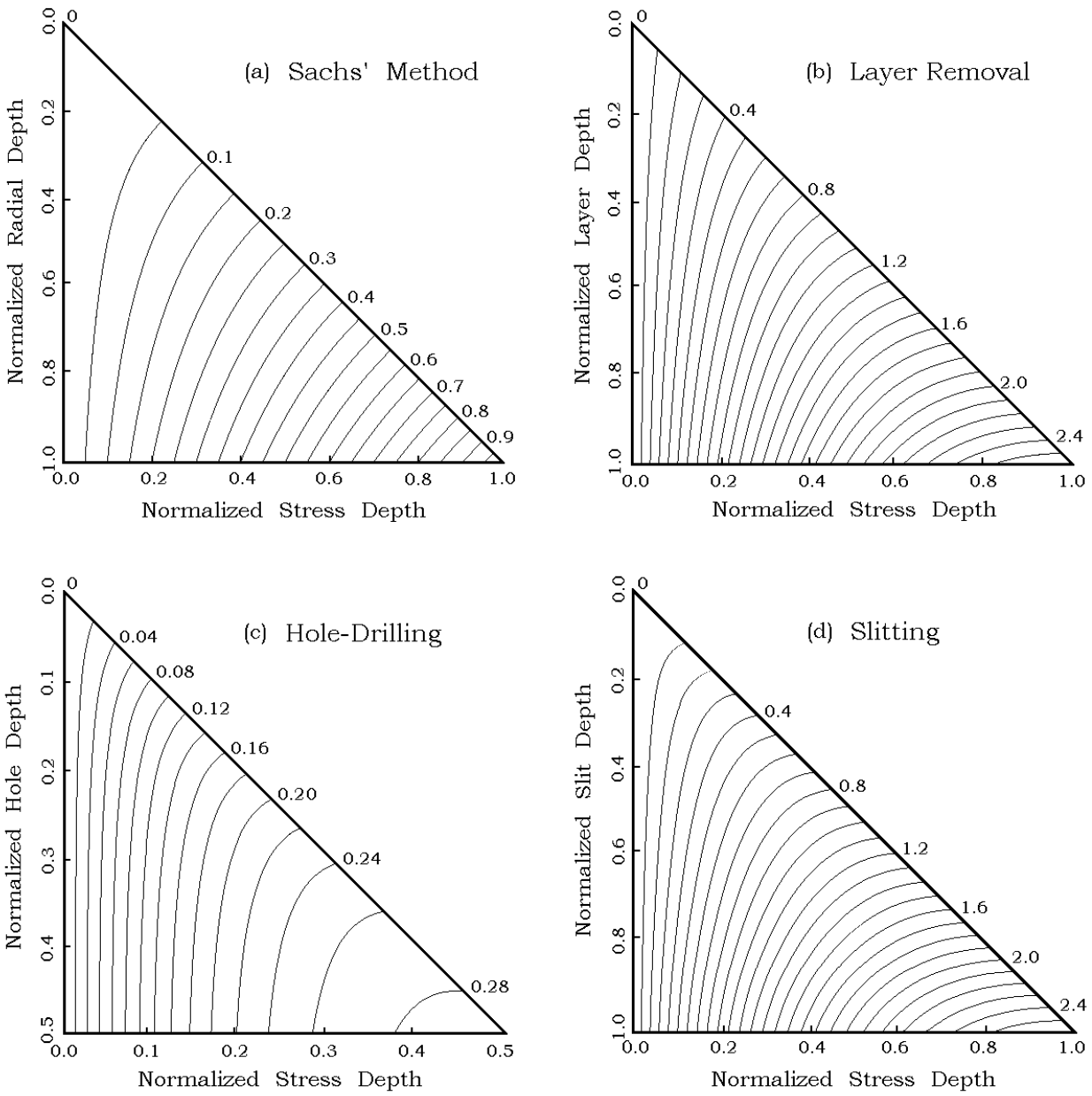

Fig.1. Contour plots of kernel function integrals. (a) Sachs' Method, (b) Layer Removal, (c) Hole-Drilling [10], (d) Slitting .

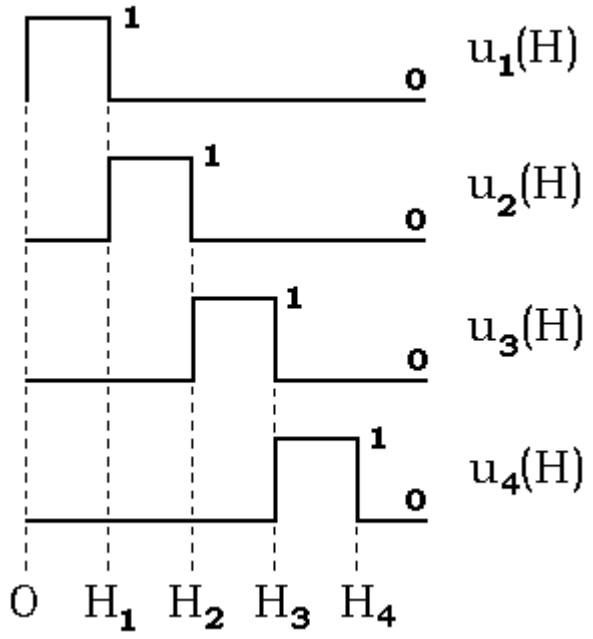

Figure 2. Unit pulse functions used for the residual stress solution.

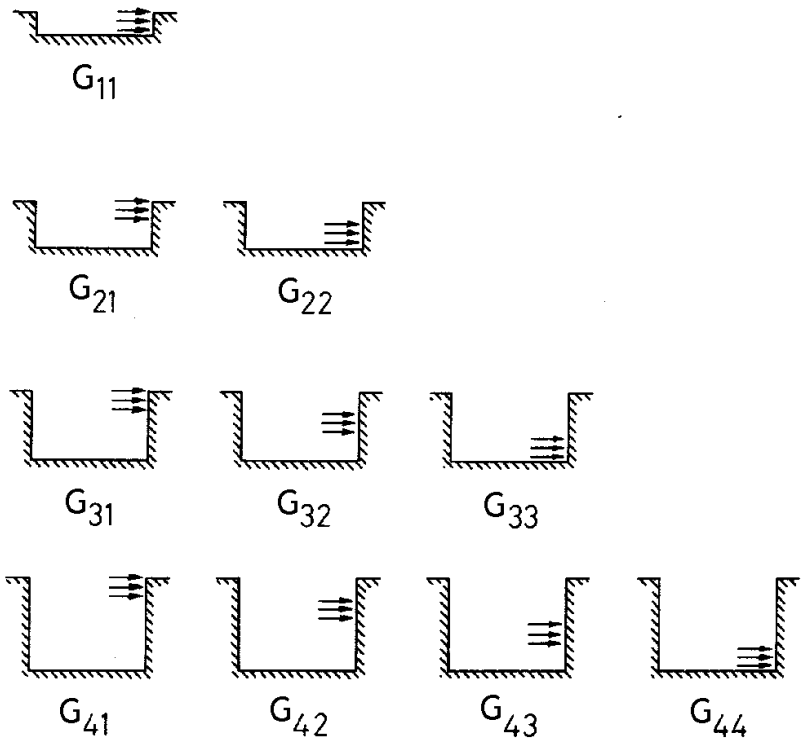

Figure 3. Physical interpretation of matrix coefficients G_{ij} for the Hole-Drilling method.

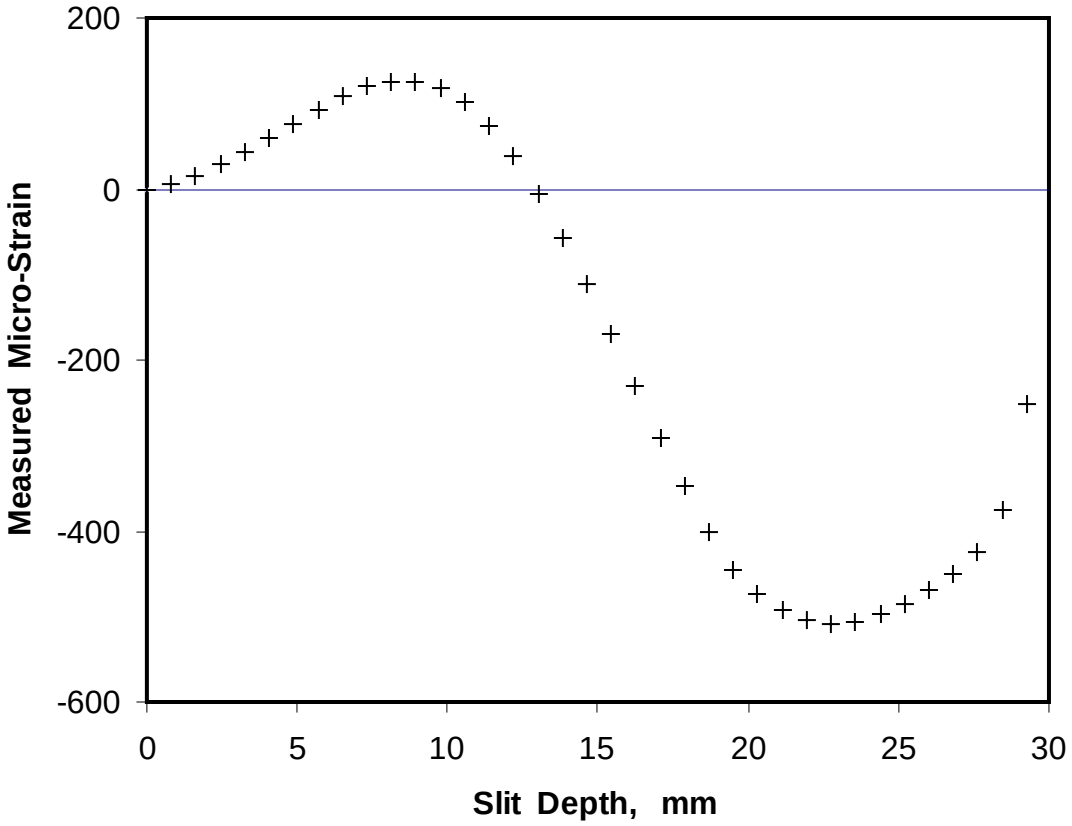

Figure 4. Strain vs. slit depth for a residual stress measurement using the Slitting method.

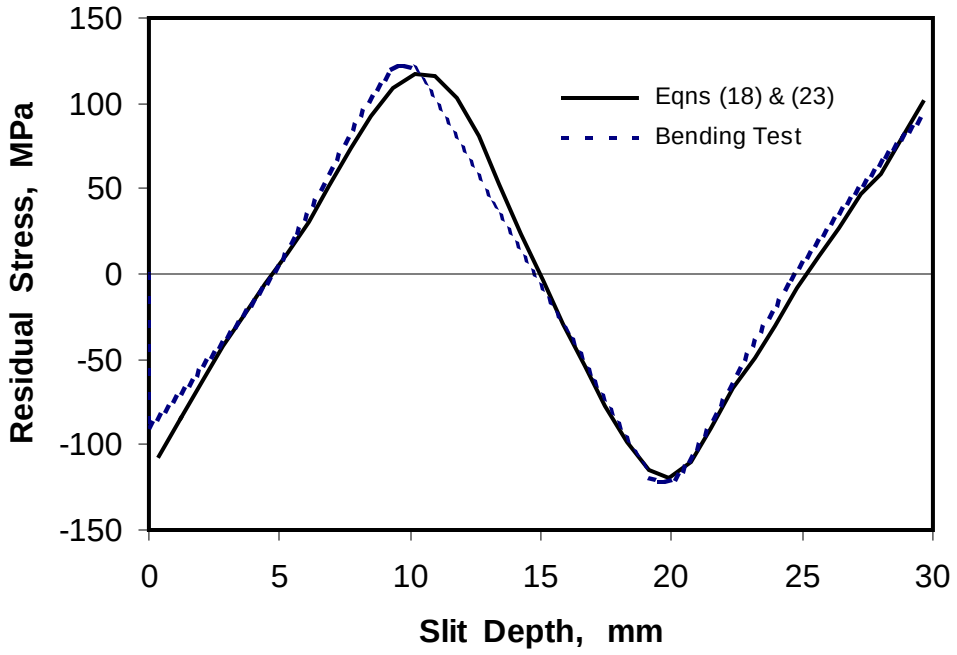

Figure 5. Residual stress profiles. Solid line = calculated from Fig.4 data using Equations (18) and (23). Dashed line = calculated from bending strains.

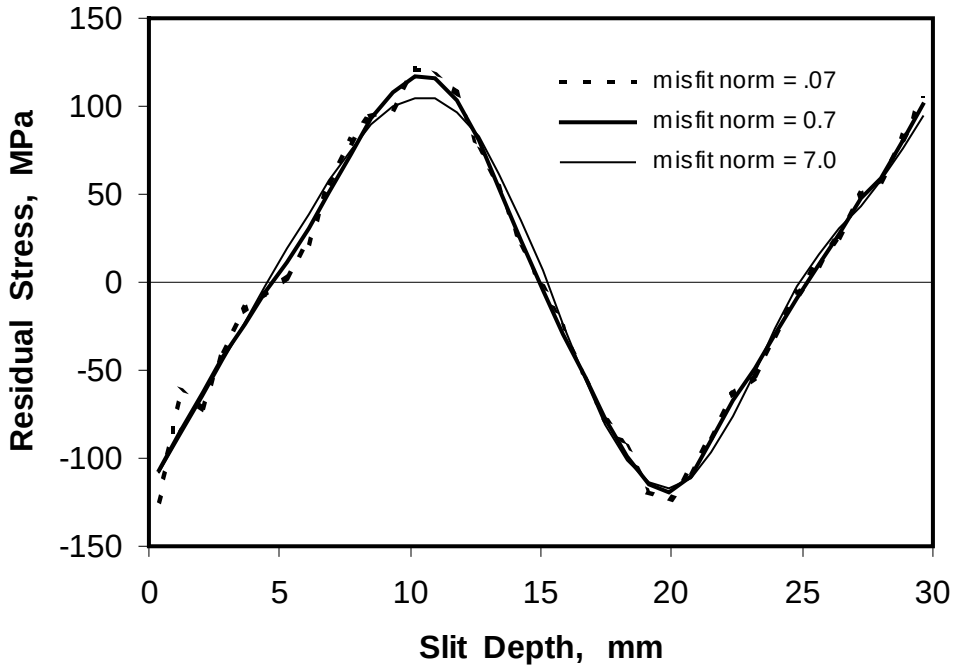

Figure 6. Residual stress profiles calculated using different amounts of regularization. Misfit norms = 0.07, 0.7 (optimal) and 7.0 micro-strain.

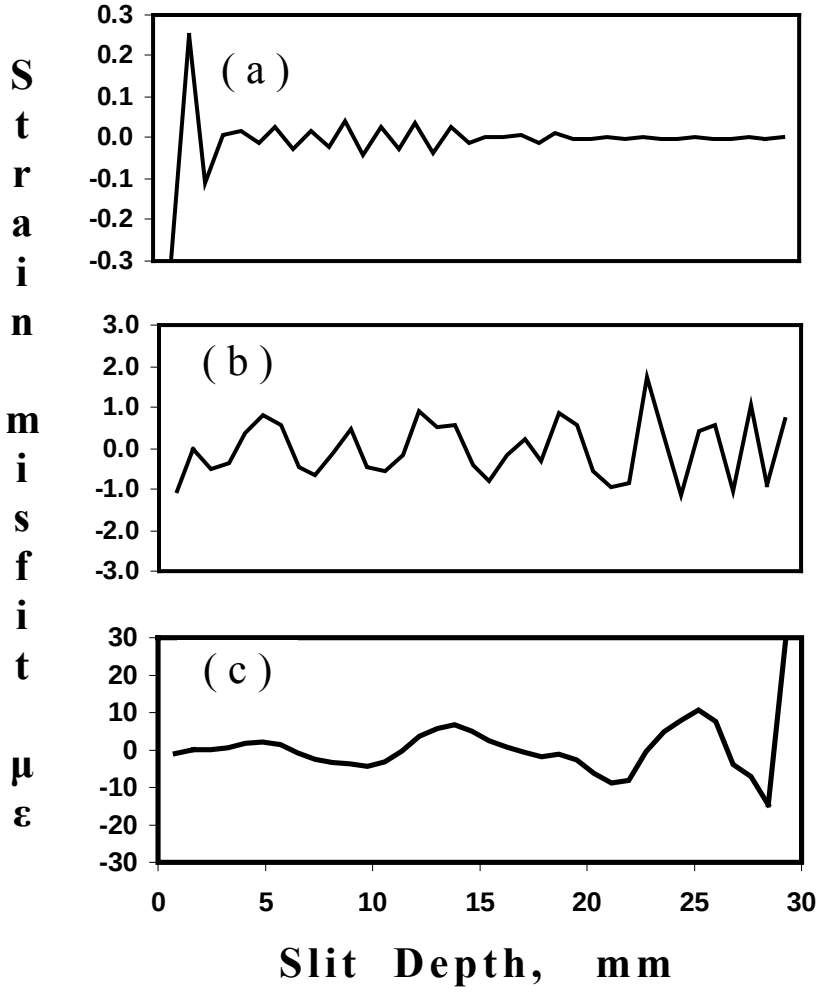

Figure 7. Strain misfits calculated using different amounts of regularization. Misfit norms: (a) = 0.07, (b) = 0.7 (optimal), and (c) = 7.0 micro-strain.